Journal of Membrane Science 500 (2016) 124–135

Contents lists available at ScienceDirect

Journal of Membrane Science

journal homepage: www.elsevier.com/locate/memsci

Impact of liquid-filled voids within the active layer on transport through thin-film composite membranes

Mavis C.Y. Wong [a], Lin Lin [b], Orlando Coronell [b], Eric M.V. Hoek [a,1], Guy Z. Ramon [c,*]

[a] Department of Civil & Environmental Engineering, University of California, California NanoSystems Institute and Institute of the Environment & Sustainability, Los Angeles, CA, USA

[b] Department of Environmental Sciences and Engineering, Gillings School of Global Public Health, University of North Carolina at Chapel Hill, Chapel Hill, NC, USA

[c] Department of Civil & Environmental Engineering, Technion – Israel Institute of Technology, Haifa, Israel

ARTICLE INFO

Article history:
Received 30 July 2015
Received in revised form
11 November 2015
Accepted 22 November 2015
Available online 2 December 2015

Keywords:
Composite membrane
Reverse osmosis
Nanofiltration
Membrane transport
Solution-diffusion
Fouling

ABSTRACT

Transport through composite membranes is strongly influenced by the morphologies of both the porous support membrane and overlying selective thin-film (i.e., active layer). Recently, the occurrence of water-filled voids within the active layer has been suggested in the literature; however, their effects on transport are uncertain. Here, we theoretically consider, through numerical modeling, the effect that liquid filled-voids have on the transport of water and solutes through supported thin-film morphologies. Specifically, we evaluated the effect of volume void fraction, void size, and relative location of the voids within the active layer with respect to both surface roughness features and the pores of the support. Transmission electron microscopy image analysis was used to obtain evidence supporting the existence of voids in two commercial brackish and seawater reverse osmosis membranes; the volume fraction of the active layer the voids occupied was determined to be about 30% for both membranes. Our calculations show that, for films with a constant polymer volume, a rough film containing voids is more permeable than an equivalent, homogeneous flat film, due to the creation of shorter paths for diffusion, not due to increased surface area, though the latter is shown to correlate positively with permeability when no base-film exists under the void. Results further illustrate the importance of void position within the thin-film, indicating that even with a significant void fraction, the presence of an underlying polymer base-film negatively impacts the permeability. Voids created closer to the bottom of the active layer will increase membrane permeability. Conversely, results show that even at significant void fractions, voids located closer to the top of the active layer negatively impact the permeability. Variations in the proportion of the active layer overlaying the voids will impact the flux distribution along the membrane, and may be used to reduce flux 'hotspots', which may enhance localized concentration polarization and fouling propensity. A strategy for creating high permeability membranes with relatively even flux distributions may include a combination of a rough film with a reduced base thickness, and with thicker regions of the film aligned with the support pore locations. Understanding the role of the voids in determining the transport properties of the membranes provides motivation for controlling their formation.

© 2015 Elsevier B.V. All rights reserved.

1. Introduction

State-of-the-art reverse osmosis (RO) and nanofiltration (NF) membranes are comprised of an ultra-thin polyamide film formed over a porous support membrane (typically polysulfone cast over a polyester non-woven fabric). Despite their dominant role in the water purification, reuse and desalination industry, basic questions of how the morphology of the support (e.g., porosity, pore size, structure and distribution) and of the thin-film impact transport through the composite membrane, and the consequent implications on membrane fouling propensity, have not received much attention in the open literature. Classical treatment of membrane transport, e.g. within the framework of the solution-diffusion model [1], is normally employed with the assumption of a homogeneous film of uniform thickness. Recent modeling efforts have extended this framework to consider the effects of the porous support as well as a non-uniform film thickness [2–4], illustrating

* Corresponding author.
E-mail address: ramong@technion.ac.il (G.Z. Ramon).

[1] Current address: Water Planet, Inc., 721 S. Glasgow Ave., Los Angeles, California, 90301, USA.

http://dx.doi.org/10.1016/j.memsci.2015.11.033
0376-7388/© 2015 Elsevier B.V. All rights reserved.

the pronounced effect on transport of purely geometrical considerations, unaffected by polymer chemistry, which is assumed to be constant within the model framework. This assumption facilitates the de-coupling between the polymer chemistry and the film morphology-these appear to be intimately linked, yet are not very well understood. When considering identical monomers from which the polymer backbone is created, it has been demonstrated that the polyamide permeability may be modified through the interfacial polymerization conditions; these include temperature, choice of solvents, monomer concentrations, co-solvent additions and the properties of the support membrane, to name a few [5–9]. These conditions also impact the film morphology; therefore, it is important to remember that the assumption of keeping constant polymer properties (i.e., as embodied in parameters such as partitioning and diffusivities of permeating species) while changing the morphology cannot depict the full, complex picture. A recent study has demonstrated that, even after accounting for some geometrical considerations, variations in transport properties still exist [10]. Separating the effect of geometry from chemistry in an experimental setting is difficult (if not impossible); thus, model simulations afford us the luxury of probing geometrical effects separately, so as to shed insight on their relative impact and motivate further attempts at their manipulation.

Experimental work has previously attempted to correlate the roughness of RO membranes with their permeability, with some suggesting that an increased permeability is to be expected due to roughness-increased surface area; these studies obtained mixed results, showing no clear correlation [9,11–14]. Theoretically, it has been shown that roughness can only increase permeability if it is created via a redistribution of polymer into thin and thick parts [3]. However, the previous theoretical efforts have assumed that the thin film is comprised of a homogeneous polymer. The question may be raised – is this indeed the case and, if not, what would be the impact of a non-homogeneous structure? This question is also motivated by recent advances in higher resolution imaging that have allowed improved characterization of RO and NF membranes revealing, in detail, the thin film morphology. A representative collection of recently published images is compiled in Fig. 1, highlighting the globular features and rough morphology of RO membrane thin films. Scanning Electron Microscopy (SEM) surface images of RO membranes (Fig. 1a) show the "ridge and valley", "leafy protrusions" or "carpet-like" morphology typical of fully aromatic polyamide films. Transmission Electron Microscopy (TEM) images (see Fig. 1b–d) show that the films are not uniform in composition, with regions of dense polymer film and regions of what appear to be open voids or regions of lower polymer density. A few research groups have observed this structure in RO thin films [15–19], that is, a dense basal region near the support layer, overlain by polymer leafs surrounding globular voids, and it has recently been demonstrated that these voids are fluid-filled when immersed in water [10]. The introduction of hollow, fluid-filled domains within the thin film and possibly between the film and support membrane raises interesting questions with respect to transport mechanisms through composite NF/RO membranes.

We note that a first approximation of transport through a polymer containing voids seems quite straightforward, using results from 'effective medium theory' [20]. A polymer film of a given permeability, containing liquid voids that may be considered as having much higher permeability, will be more permeable than the pure polymer phase. However, this theoretical framework is limited to non-interacting inclusions; in other words, the liquid-filled voids must be far apart, and cannot amount to a significant fraction of the total volume ($<10\%$). Furthermore, the effective medium theory cannot specifically account for the effect of the porous support as well as geometry and spatial distribution, e.g. whether voids are located close to the film-support interface, whether they are close to support pore locations, etc. Clearly, a more elaborate calculation is needed to better understand the effect of the voids on the permeation of water and solutes for the composite structure and morphological features relevant to NF/RO membranes.

Apart from impacting permeability, film morphology has also been linked to fouling propensity. For example, experimental evidence suggests that colloidal fouling is lower for smooth, integrally-skinned cellulose acetate RO membranes, compared with that observed for rough, thin-film composite membranes (see, for example, [21,22]). While this observation has been explained primarily using arguments related to hydrophilicity, recent theoretical studies of transport through composites have also suggested that increased fouling propensity may be induced by flux 'hot-spots', that is, regions of greatly increased permeability, where initial deposition is expected to occur [2,3]. These hotspots have been shown to result via three main contributions: (1) thin-film thickness; (2) variations in film thickness (i.e., roughness) and their relative positioning with respect to support pore locations; and (3) the permeability of the solid make-up of the support

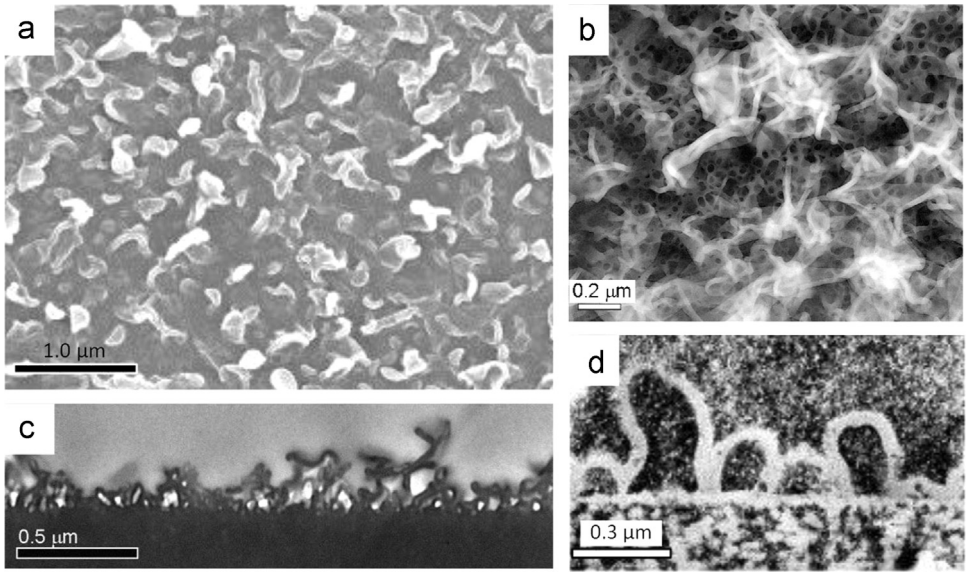

Fig. 1. (a) Surface SEM [8], (b) top view [9] and (c/d) cross-sectional TEM images [9,10] of polyamide RO membrane thin films, collected from the published literature.

structure [2,3]. All three contributions act in favor of reducing hotspot occurrence and intensity in cellulosic membranes, illustrating that hydrophilicity, though certainly of importance, is by no means the sole contributor to their reduced fouling propensity. If the presence of liquid-filled voids within the thin film modifies the permeability of the composite, then it stands to reason that the flux distribution will also be altered, but it is not clear to what extent. If, indeed, increased permeability comes at the cost of exacerbated fouling propensity, knowledge of such an interplay may inform better design; in this case, the presence of voids and the manipulation of their distribution and size potentially offer additional degrees of freedom enabling maximizing permeability at a minimum increased fouling propensity.

In what follows, we present a first attempt to probe the impact of fluid-filled voids on the permeability of the thin film (i.e., active layer) as well as the composite (i.e., supported thin film). We use a numerical model, complemented by transmission electron microscopy image analysis of two commercial membranes. Specifically, the objectives of the study are: (1) to assess the altered permeability of films containing liquid-filled voids (modeled as inclusions of highly permeable material), as a function of void size and location within the film; (2) to gauge the impact of the modified transport paths through the composite on the flux distribution over the membrane surface; and (3) to discuss the potential trade-off between increased permeability and fouling propensity (due to occurrence of flux hotspots), towards balancing the two effects in the presence of voids within the thin film.

2. Theory

2.1. Model geometrical framework

In the spirit of previous studies [2–4], we use idealized, periodic structures to mimic the uneven coating film thickness and the underlying support pore locations. While this is certainly not the true morphology of such membranes, it must be realized that true surface morphologies are random, as are the support pore size and distribution. This leads to the conclusion that any attempt to truly mimic the possible combinations would result in an extremely large parameter space. More importantly, there is little assurance that even such extensive calculations would be quantitatively predictive. Therefore, we choose a simplified framework whose main assumption is periodicity of both film morphology (roughness) and support pore distribution. The assumption of periodicity is used extensively in mathematical modeling of heterogeneous systems, since it leads to physically insightful results even in complex situations, despite the fact that 'real' systems are seldom periodic [23]. As pointed out by Bruna et al. [4], the deviation of calculations made for periodic structures from averaged random distributions is quite small. The periodic structures used here aim to capture essential features in a simple-to-grasp manner and with a minimized parameter space.

To fix ideas: a sinusoidal wave with varying amplitude is used to emulate the rough morphology of the polyamide thin film. Liquid-filled voids are introduced into the film as domains with different material properties. Support pores located directly underneath roughness minima (valleys) are defined as "in-phase" with roughness, whereas pores aligned with roughness maxima are defined to be "out-of-phase"; simulations performed without accounting for the support are referred to, appropriately, as "unsupported". A schematic of the model geometries illustrating these definitions is shown in Fig. 2. This framework allows one to consider how variations in thin film thickness as a function of void size and location impact permeability, and how that interacts with the position of pores in the underlying support. As shown by Ramon and Hoek [3], the interaction between thin film thickness and support pores location can lead to increased or decreased flux, as well as enhancement or dampening of flux variability over the membrane surface. Inclusion of the voids in the thin film morphology, will allow for an evaluation of how the voids size and location affect this enhancement or dampening of flux variability. The consideration of extreme cases (in and out of phase) is adopted since when the variation between two points is monotonic, no insight is gained by considering the intermediate combinations.

The characteristic size of morphological features involves a 'base' film thickness, t_b, (see Fig. 2) which we take to be the thickness of the polymer region between the support and voids; we further define a scaled roughness amplitude, R_f, which is the ratio of the sinusoidal wave amplitude, R_a, to the base film thickness, or $R_f = R_a/t_b$. Available literature data suggests that typical RMS roughness features for an RO membrane range between ~50 and 180 nm [24–26]; average pore sizes of support membranes are in the range 5–30 nm [12,27] and surface porosity has been reported to be in the range 1–5% [27]. Based on published AFM data, the size of roughness protrusions above the lowest point (which is the location of the 'base-film' here) varies widely between different membrane types, and can be up to ~1 μm [25]; however, on average these values appear to vary between ~50 nm and ~300 nm for a range of RO membranes [24–26]. From SEM and TEM images, the base film thickness ranges from 10 to 100 nm; hence, the scaled roughness amplitude R_f, as defined here, is typically greater than unity, on average, and can locally be greater

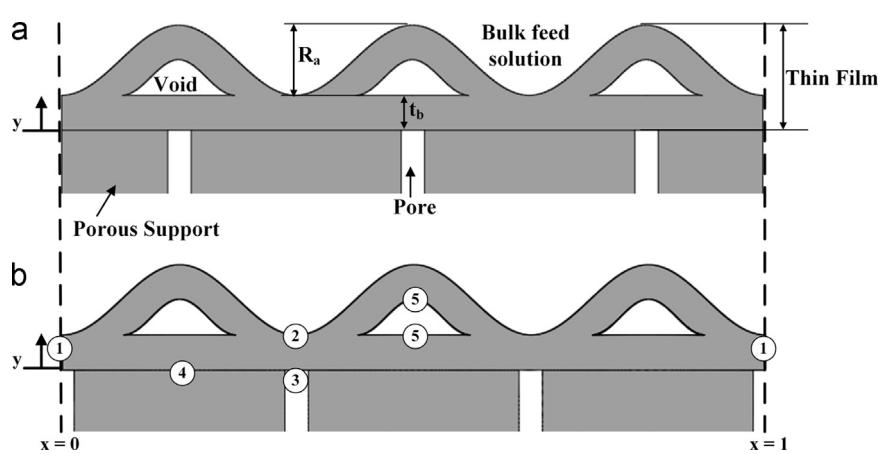

Fig. 2. Schematic of geometry used in simulations for (a) out-of-phase and (b) in-phase supported membranes (number labels correspond with the boundary conditions referred to in Table 1).

than ~10. In light of these representative values, film morphology was modeled with a wavelength (peak-to-peak separation) of 200 nm, a base film thickness of 50 nm (essentially an average of 100 nm, varying sinusoidally between 50 and 150 nm), and a scaled roughness amplitude of 1–5. The support membrane top surface was modeled with pore diameter of 10 nm and porosity of 2%. We also note that, strictly speaking, separation and wavelength of the active layer roughness merely represent the length scales over which the active layer thickness varies. The void fraction was changed either independent of or proportionately with the roughness (since voids are assumed to be a consequence of the film formation process). The range of void fractions generally corresponds with TEM image analysis, as will be discussed in Section 4.1 However, it is used to simply ask the question of what a low or high void fraction does to the transport properties of the membrane.

2.2. Governing equations

Within the thin-film, and consistent with the solution-diffusion framework, we consider steady-state diffusion governed by a two-dimensional Laplace equation, viz.

$$\nabla^2 C_i = 0, \tag{1}$$

in which $\nabla=\{\frac{\partial}{\partial X}, \frac{\partial}{\partial Y}\}$, X and Y are the usual Cartesian coordinates, and C_i is the concentration of the diffusing species. The subscript i denotes the various domains: the thin-film (f), the fluid-filled voids (v) and the support solid matrix (s). The 2D simplification is based on prior results that indicated that the deviation from 3D is not significant, which motivated the greater convenience offered by a 2D simulation [2]. The concentration, c, is scaled using the bulk feed and permeate concentrations, c_b and c_p, respectively, so as to make it unity and zero at the feed and permeate interfaces: $C = (c-c_p)/(c_b - c_p)$; it is further noted that this scaling does not imply complete rejection of the solute by the membrane. Accordingly, the boundary conditions applied are that of unity at the boundary between the film and bulk feed solution, and zero at the interface between the film and support pore; this assumes a complete sink at the pore interface, based on the large disparity between the transport rates in the solid polymer and the pore fluid. Further, flux continuity is applied at the boundaries between the solid phases (film and support solid matrix), and between the film and fluid-filled voids. However, it is assumed that the support solid has significantly lower diffusivity for the permeating species (i.e. $D_s/D_f \to 0$), compared with the thin-film, resulting in a finite but very small flux at this interface; this is deemed typical of currently used materials (for the impact of relaxing this condition, see Ramon et al. [2]). In contrast, the diffusivity in the voids, once again motivated by the much larger transport rate expected in a fluid, is set at $D_v/D_f = 100$. Making this ratio larger does not significantly change the results. We do not consider a range of D_v/D_f ratios since such a change would only alter the magnitude of the permeability, not the trends observed with the size and relative position of the voids (this conclusion may also easily be inferred from 'effective' medium theory [20]). Finally, symmetry conditions are imposed on all remaining boundaries. For further clarification, all boundary conditions described above are summarized in Table 1 and labeled in Fig. 2b.

2.3. Computed results

The Laplace equation, supplemented with the boundary conditions listed in Table 1, was solved numerically using the software package COMSOL Multiphysics (version 3.5a), which employs the finite element method. A direct solver was used to invert the matrix of the algebraic equations resulting from the discretization, since it provides the fastest computation. The main computation output from the model is the concentration field within the film, from which a flux may be calculated and integrated along a boundary, for example along the film-feed interface, to obtain an average flux. Since calculations are made at a constant driving force, averaged fluxes are interpreted as permeabilities. Results are plotted against the scaled roughness amplitude, R_f, or, alternatively, against the void fraction, ϕ, defined as the ratio of the void area to the film area, expressed as a percentage.

For the first set of calculations (see illustration in Fig. 3), we wanted to evaluate the effect of the presence of the voids on the permeability and flux distribution through the thin film. A 'solid' (i.e., $\phi = 0$), rough film was included as the simplest case (Fig. 3, top), where the roughness was increased proportionally to the base film thickness. This may represent the case when a larger amount of material is involved in the reaction and, consequently, more polymer is formed. We also studied a 'constant void' scenario (Fig. 3, middle) in which a void is introduced into the film, with a maximum thickness equal to half that of the base film. In this set of calculations, the roughness amplitude of the thin film is increased while maintaining a constant void volume, thereby decreasing the void fraction. A 'proportional void' case (Fig. 3, bottom) was also studied, in which the voids are increased proportionately with the roughness amplitude such that the polymer mass (or area) is kept constant, effectively increasing the void fraction concurrently with roughness.

In a second set of simulations, we wanted to probe the way in which the relative location of a void, within the film cross-section, impacts the permeability and flux distribution. In geometrical terms, this translates to the question of whether the portion of the polymeric film overlaying a void (i.e., the top film) is thicker or thinner than the portion of the film underneath the void (i.e., the base film). Referring to Fig. 4 as a guide, case A describes the increase in the void volume by extending the bottom of the void, thereby decreasing the average thickness of the base film; in case B, the void volume is increased at the expense of the top film thickness, while in case C, the void volume is increased by decreasing both the top and base film thicknesses. For cases A, B and C, the scaled roughness amplitude is constant (at R_f=2) and hence the surface area is too, while the void fraction is increased. Of course, in reality, films are likely a random and complex combination of these scenarios, but for clarity and conciseness of analysis, simulations were kept separate in order to highlight different contributions.

Table 1
Summary of boundary conditions used in the simulations.

Boundary condition	Location	Condition[a,b]	Description
1	$X=0$, $X=1$	$\frac{\partial C_f}{\partial Y}=0$	Symmetry
2	Film/Bulk interface	$C=1$	Unity potential
3	Film/Pore Interface, Support/Pore Interface	$C=0$	Zero potential
4	Film/Support Interface	$D_f\frac{\partial C_f}{\partial Y}=D_s\frac{\partial C_s}{\partial Y}$	Flux continuity
5	Film/Void Interface	$D_f\frac{\partial C_f}{\partial Y}=D_v\frac{\partial C_v}{\partial Y}$	Flux continuity

[a] $C = (c - c_p)/(c_f - c_p)$ is the scaled concentration, c_f is the feed concentration and c_p the permeate concentration.
[b] X and Y are the scaled horizontal and vertical coordinates as labeled in Fig. 2.

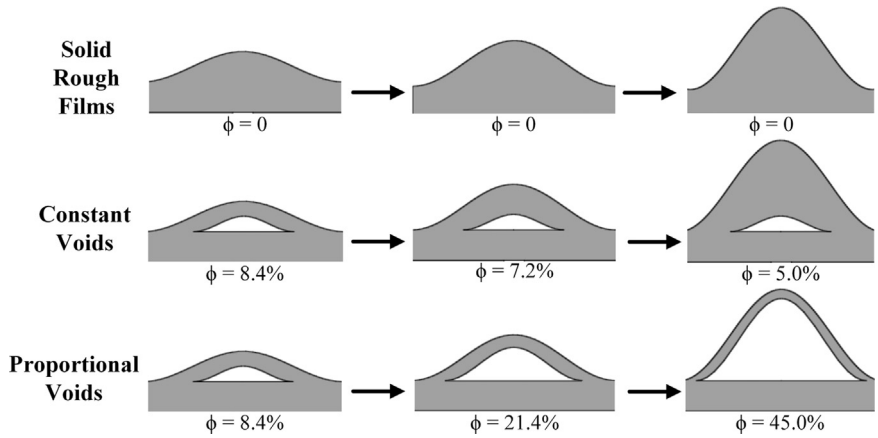

Fig. 3. Schematic depiction of the constant void and proportional void cases compared to the solid rough films, showing the corresponding void fraction for each case. A detailed definition of the constant void and proportional void cases can be found in Section 2.3.

2.4. Scaling and presentation of computed results

In a previous study [3] aimed at understanding the effect of roughness on permeability, unsupported undulating thin films were modeled, and their permeabilities were scaled against that of a flat membrane having the thickness of the base film. In such cases, the permeability of the membrane decreases as more polymer is added to increase roughness [3]. In addition, permeabilities were also scaled against that of a flat film of equivalent polymer volume, which illustrated that roughness increases the permeability only if it is a re-distribution of the polymer – creating thick parts also creates thin parts (see Fig. 5). Here, we follow a similar idea to the latter scaling approach so that the reference is taken to be the permeability of an equivalent amount of polymer distributed as a smooth flat film. Again, this scaling is used to basically ask whether, for a given case, changing the morphology of the membrane (through roughness and voids) improves the transport properties with respect to a flat, homogeneous film.

A second scaling approach in this study is taken to be with reference to the permeability of a flat film with an equivalent *total* volume (illustrated in Fig. 5), that is, the flat film resulting from a redistribution of a rough film, *including* the void volume, if present. So, in the case of a void fraction of zero, the two scaling approaches converge. The purpose of these different scaling approaches is to probe the way that polymer distribution impacts the permeability of a membrane, while highlighting the relative impact of the voids on the permeability in a self-consistent manner. The scaled permeability is denoted as P. In addition, where applicable, the permeabilities were scaled against the permeability of a solid (i.e., voidless) film with identical total volume and roughness. These choices enable a comparison to be made based on two contributions, namely, the presence of voids and the roughness, both of which impact transport through the active layer. To summarize, the scaling approaches outlined above allow some measure of decoupling between the various influences on transport. The 'mapping' to a flat morphology retains the comparative effect of roughness, and the distinction between inclusion and exclusion of the voids highlights their impact. In similar fashion, the comparison with a solid film with identical roughness eliminates the contribution of roughness.

Finally, for the purpose of characterizing the flux distributions, we calculate the scaled peak flux (J_P), which is the ratio of the maximum local flux along a membrane segment and the average flux over the membrane segment. This quantity is used as a proxy for the severity of 'hotspots' created by the various geometries, with implications on membrane scaling, fouling and defect formation.

3. Experimental

3.1. Membranes

In this study, the membranes used were polyamide thin-film composite XLE and SW30HR (Dow FILMTEC™, Minneapolis, MN), marketed as brackish water and seawater RO membranes, respectively.

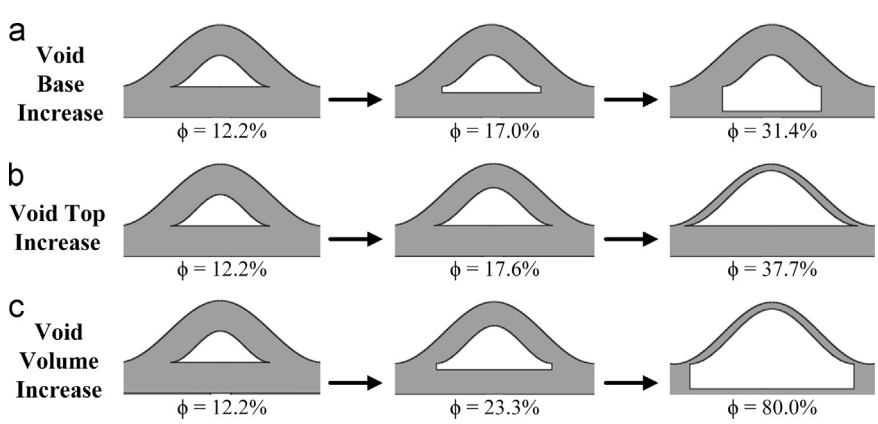

Fig. 4. Schematic of changes to void volume due to void relative location within the film, and corresponding void fraction changes. A detailed description of how void volume was changed for modeling purposes can be found in Section 2.3.

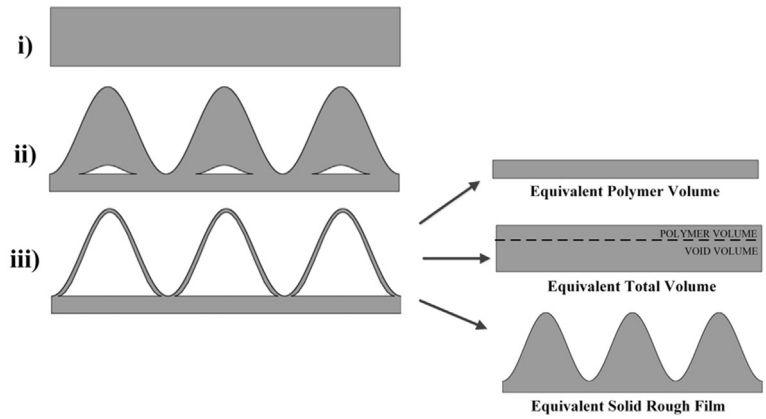

Figure	Void Fraction %	Calculated Permeability	Permeability scaled by equivalent polymer volume	Permeability scaled by equivalent total volume	Permeability scaled by equivalent solid rough film
i	0.0	5.93	1.00	1.00	-
ii	3.6	11.29	1.90	1.98	1.03
iii	60.7	17.87	1.23	3.13	1.63

Fig. 5. Schematic illustration of the scaling used to compare the active layer morphologies, and example calculations of the permeability in each case. Illustration (iii) also shows the mapping of a rough active layer that contains voids into the 3 equivalent films used for the different scaling approaches. Permeability values are scaled with respect to reference films that are either a solid flat film with equivalent polymer volume, a solid flat film with equivalent total volume (polymer and voids), or as a solid rough film with equivalent total volume, as illustrated in the inset of illustration (iii). A detailed description of the three scaling approaches used can be found in Section 2.4.

3.2. TEM analyses

TEM imaging was performed with samples prepared with a procedure similar to that reported by Tang et al. [28]. Briefly, clean $2.5 \times 5.0\ cm^2$ membrane coupons were dried with filter paper and subjected to three 15-min cycles of dehydration with fresh 100% ethanol (Fisher Scientific, Pittsburgh, PA). After dehydration, LR White resin (London Resin Co, Reading, UK) diluted in ethanol at different volume-to-volume ratios was used to infiltrate the samples in four steps lasting 1 h (50%v/v), 2 h (67%v/v), 3 h (100% v/v) and 2 h (100%v/v), respectively. Next, the resin was cured at 48 °C for 3 days, and the samples were sliced to a thickness of approximately 90–100 nm using an ultramicrotome. The resulting 90–100 nm thick specimens were used to obtain cross-sectional TEM images using a JEOL 100CX II TEM (JEOL USA, Peabody, MA) at an accelerating voltage of 80 kV and magnification of 29,000–72,000 ×. The software ImageJ (Image J, version 1.47v [29], http://imagej.nih.gov/ij/) was used to analyze the TEM images to obtain the areal fraction of the active layers occupied by the voids in each membrane. The areal void fraction was calculated as the ratio between the area of the voids in the active layer and the total area of the active layer as measured with ImageJ. The values reported in this study for each membrane correspond to the average and standard deviation of results for three images.

4. Results and discussion

4.1. Presence of voids and void fraction in active layers

Representative cross-sectional TEM images of the XLE and SW30HR membranes are shown in Fig. 6. The images outline in red the area corresponding to the active layers thin film and indicate with white arrows the globular features believed to be voids. Both images show that the voids are present in the active layers and have characteristic sizes ranging from a few tens to a couple of hundreds of nanometers, encompassing the size range (20–60 nm) reported by Pacheco et al. [14] for the globular features observed in the active layers of the ESPA3 membrane (Hydranautics, Oceanside, CA).

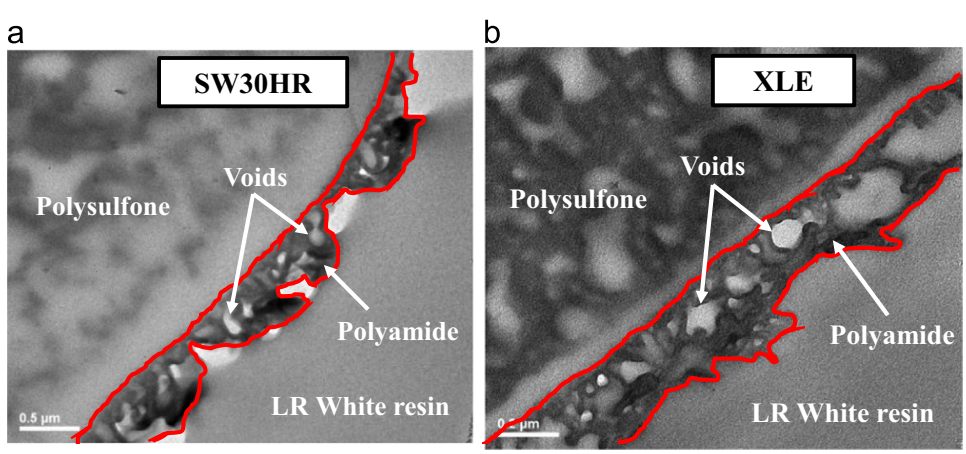

Fig. 6. Cross-sectional TEM images of samples of the XLE (a) and SW30HR (b) membranes. For each membrane, the perimeter of the polyamide thin-film is outlined in red, and examples of voids in the active layer are indicated by arrows.

Through visual inspection, the images also indicate that the areal fraction of voids in the active layers is not negligible. The areal void fraction, estimated using the ImageJ software, were $32 \pm 4\%$ and $30 \pm 6\%$ for the XLE and SW30HR membranes, respectively, confirming that the void fraction is significant. This data is consistent with a companion study that showed - through comprehensive experimental characterization – that the void fraction of aromatic polyamide active layers in NF, brackish water and seawater RO membranes was in the range of $15 \pm 2\%$ to $32 \pm 4\%$ [10]. It appears reasonable to assume that the voids are *not* connected to each other and/or to the feed sides of the membrane. This assumption is consistent with the inability to observe clear connections between voids in TEM images, and is also supported by TEM images of material deposited on top of RO membranes, which appears to be entirely captured above the thin film and not within the voids [15,30]. Connectivity to the permeate side has been suggested in recent studies [14,15,19], and is one of the scenarios investigated computationally herein, particularly in Section 4.4.

4.2. Impact of roughness, void fraction and void location on permeability

In the model geometry (as depicted in Figs. 2–4) inspired by the TEM cross-section images, the permeating species (e.g. salt/water) first diffuses from the bulk fluid on the feed side through the top polymer film, then possibly through a fluid-filled void in which it has a much higher diffusivity, and finally through the base polymer film prior to reaching the bulk fluid on the permeate side of the membrane. In order to isolate the impact of roughness and void properties, the following calculations are made for unsupported active layers.

4.2.1. Active layers with constant and 'proportional' voids

As shown schematically in Fig. 3, we have defined cases where voids are either of a constant size (such that when roughness is increased, the void fraction decreases), or a size that is proportional to the roughness amplitude (such that when roughness is increased, the void fraction remains constant). Fig. 7a shows that for active layers with varying roughness, the permeabilities of both the constant and proportional void scenarios trend similarly, increasing with roughness, when scaled against active layers with equivalent polymer volume or equivalent total volume. As discussed previously, this is because by creating a rough film, the valleys provide shorter diffusion paths compared to an equivalent smooth film. The permeability enhancement for the constant void case is larger than the proportional voids, when scaled against the total polymer volume. Here, the impact of a small void has a greater impact than a large one, provided that there is a significant polyamide film under the void – this 'base' film then sets the limit to transport (see also concentration and diffusive streamline plots, Fig. S1, in the supporting information). Fig. 7a also shows that for the proportional void case, the increase in permeability with increasing roughness has the same slope when scaled by the membrane with equivalent polymer volume and the membrane with equivalent total volume. This is because regardless of the roughness, the two membranes have the same polymer volume. The constant polymer volume may also be used to explain the more modest increase in permeability of the proportional void case compared with the constant void case, where the added polymer contributes to a growing gap between the permeability achievable through a better distributed rough film with voids and a flat, increasingly thicker, film. We note that an inflection point is observed at scaled roughness amplitude of 1 (that is, roughness amplitude at equal thickness as the bottom film), which corresponds to the point where a void is first introduced into the film, causing a shift in the permeability.

Fig. 7b shows the permeability of constant void and proportional void scenarios plotted against void fraction. For the proportional case, the permeability increases with void fraction similarly to when plotted against scaled roughness since the void fraction increases with roughness. In contrast, for the constant void case, the permeability increases with decreasing void fraction compared to that of a flat solid film with equivalent polymer volume. This is because for lower void fractions the membranes consist of more polymer, and therefore the equivalent flat membrane is thicker and less permeable.

4.2.2. Effect of void location within the active layer

Fig. 8 shows the permeability of unsupported active layers for cases where the effect of void location within the polymer film is examined (designated A, B and C for voids distributed closer to the top of the film, the base film, and both, respectively, see Fig. 4), as a function of void fraction, scaled against a membrane of equivalent polymer volume. For case A, the void fraction increases by decreasing the base film, and the permeability increases monotonically. At high void volumes, the base film becomes so thin that the shortest path for diffusion is through the portion of the active

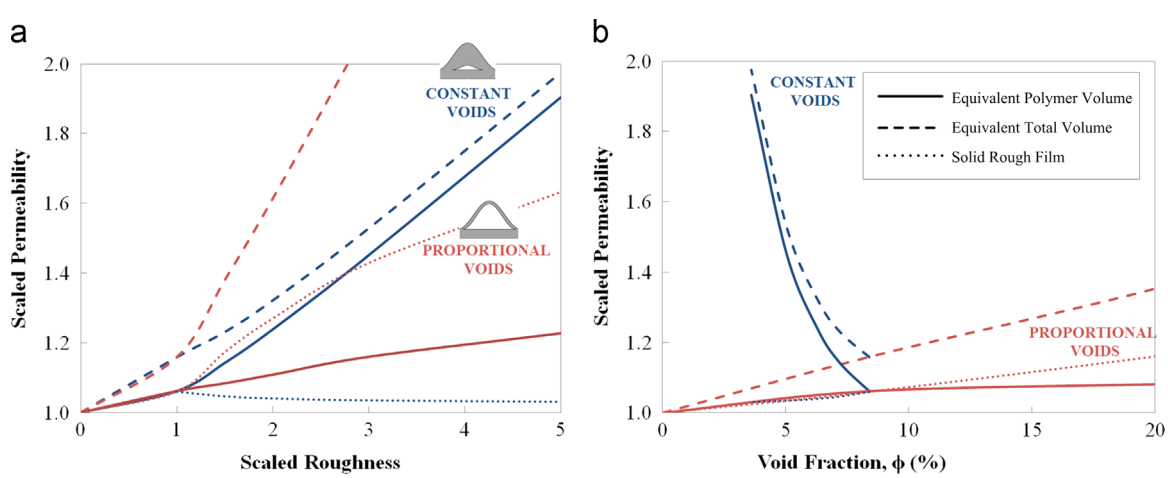

Fig. 7. Scaled permeability of an unsupported film for the constant voids (blue lines) and proportional voids (red lines) scenarios, plotted against (a) scaled roughness amplitude, and (b) void fraction. The permeabilities are scaled against either an equivalent solid film (i.e., same roughness and total volume but with no voids) (dotted lines), or a solid flat film with the same polymer volume (solid lines) or total (polymer + void) volume (dashed lines). For definitions of the different scaling methods, please refer to Fig. 3 and Section 2.3. (For interpretation of the references to color in this figure legend, the reader is referred to the web version of this article.)

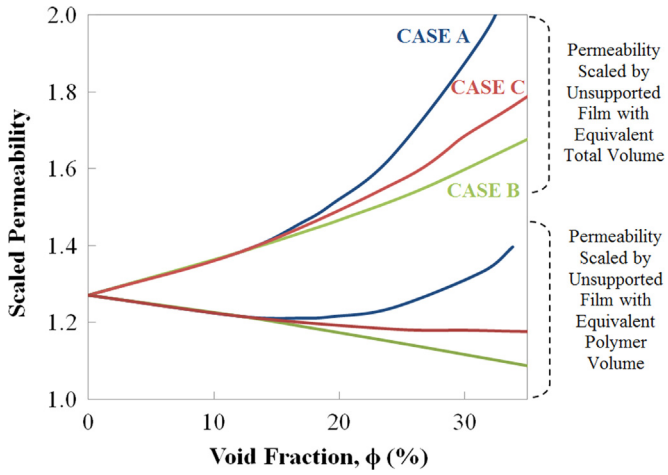

Fig. 8. Scaled permeability of an unsupported active layer for cases A, B, C (see Fig. 4), scaled against an equivalent flat film with identical polymer and total (polymer+void) volume, as a function of the void fraction.

layer overlaying the void space, then through the void, to effectively reach the bulk fluid on the permeate side of the membrane. When the thickness of the base film is reduced to almost zero, the permeability of the membrane can greatly surpass that of a solid flat film of same polymer volume-these results highlight the importance of the base film in determining the permeability of the membrane. Furthermore, this constitutes a case where *permeability will correlate positively with roughness*, due to increased surface area.

For case B, the void fraction increases by decreasing the top film thickness, and the permeability decreases as the void fraction increases. This indicates that the base film thickness has a greater impact on dictating transport resistance and thereby the permeability of the overall membrane. For case C, the void fraction increases by decreasing both the top base film thicknesses. The permeability changes minimally as the void volume increases, because case C may be viewed as a combination of cases A and B. Both effects seem to mostly balance out in the cases considered.

4.3. 'Hot-spot' creation is dominated by the support pore locations

We now turn to consider the interaction between the presence of roughness, voids and the locations of pores in the underlying support interface with the active layer. For a solid (no voids) film, as discussed previously [3], the in-phase configuration creates a much higher peak flux (J_P) than the out-of-phase one, due to the alignment of support pores with the valleys of the active layer, and this trend is monotonically positive with increasing roughness (see Fig. S1 in the Supporting material). Curiously, for the out-of-phase scenario (Fig. S1-b), there is an inflection point at which increased roughness reduces the peak flux. For low roughness, the flux is highest through the 'peaks' directly located above a pore-that is the shortest diffusion path. However, as roughness increases, the shortest diffusion paths now originate from the valleys of the film. The pivotal point for this simulation is R_f=2, where the streamlines are almost evenly distributed throughout the film, effectively minimizing the peak flux.

When voids of constant volume are added into the film, as shown in Fig. 9, the flux distributions are similar to those observed in the solid film case (Fig. S1). For the in-phase scenario (Fig. 9a), the streamlines indicate that all the flux originates from the valley directly above the pore as that location provides the shortest diffusion path. This becomes even clearer when the roughness increases and more 'dead volume' appears as the streamlines cut straight towards the pore, and no streamlines appear in the peak

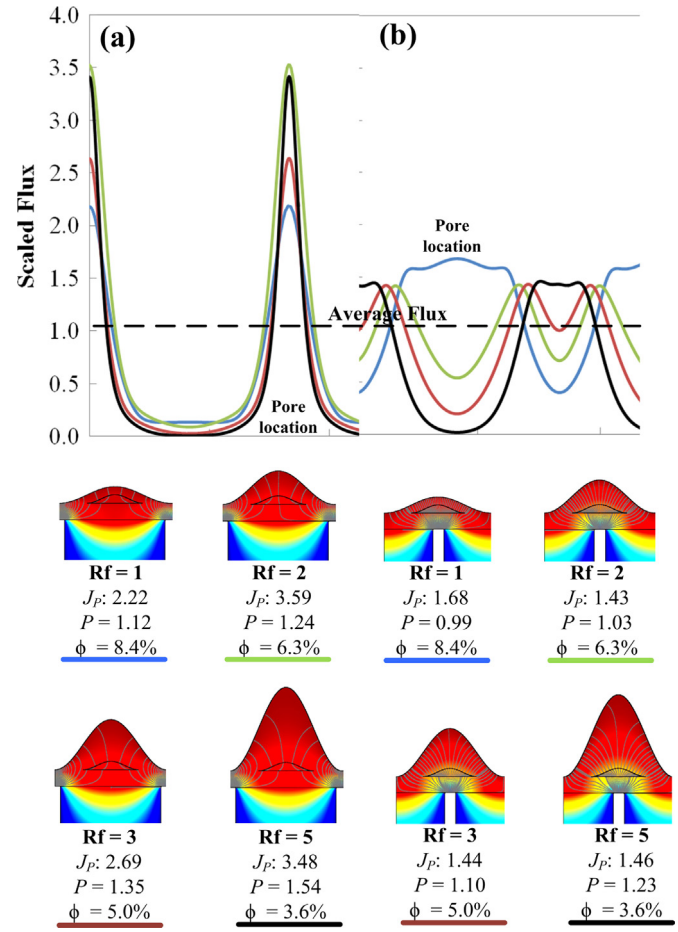

Fig. 9. Supported membranes – constant void case (see Fig. 3) with varying roughness amplitude. Pores and roughness minima (i.e., valleys) are either: (a) in-phase (aligned), or (b) out of phase. Top panel shows flux variation plots. Bottom panel shows, for each case, the concentration field, diffusive streamlines and corresponding calculated peak scaled flux, J_P and the permeability P, scaled against that of an equivalent flat thin film with an identical polymer volume.

regions of the film – these are effectively saturated and do not exhibit concentration gradients. A similar effect is noticed for the out-of-phase case (Fig. 9b) in which the void acts as a 'funnel' for flux towards the support pore but does not reduce the value of J_P. The largest resistance, or rate-limiting step for reaching the pore remains diffusion through the base film, and since the base film thickness is the same both for this case as well as the solid film case, no significant improvement in permeability is expected. This case shows that the presence of a void in the thin film does not necessarily reduce the value of the peak flux nor change the flux distribution because the distribution and magnitude of hotspots are primarily dictated by the base film thickness and support pore locations.

When the voids are proportional to the roughness of the thin film, as shown in Fig. 10, the flux variation is dramatically reduced for the out-of-phase case (Fig. 10b), similar to the solid film and constant void scenarios. However, for the in-phase scenario (Fig. 10a) the flux variability increases dramatically as the roughness increases. This is similar to the solid film - the average diffusion path decreases as roughness increases, and thus even though the permeability is practically kept constant (in contrast with the increase observed for a solid film), the scaled peak flux is large, signifying intense hotspots. Conversely, for the out-of-phase case, as roughness increases, the flux variability is reduced and the flux is more evenly distributed. This demonstrates yet again that the support membrane alignment is crucial in not only

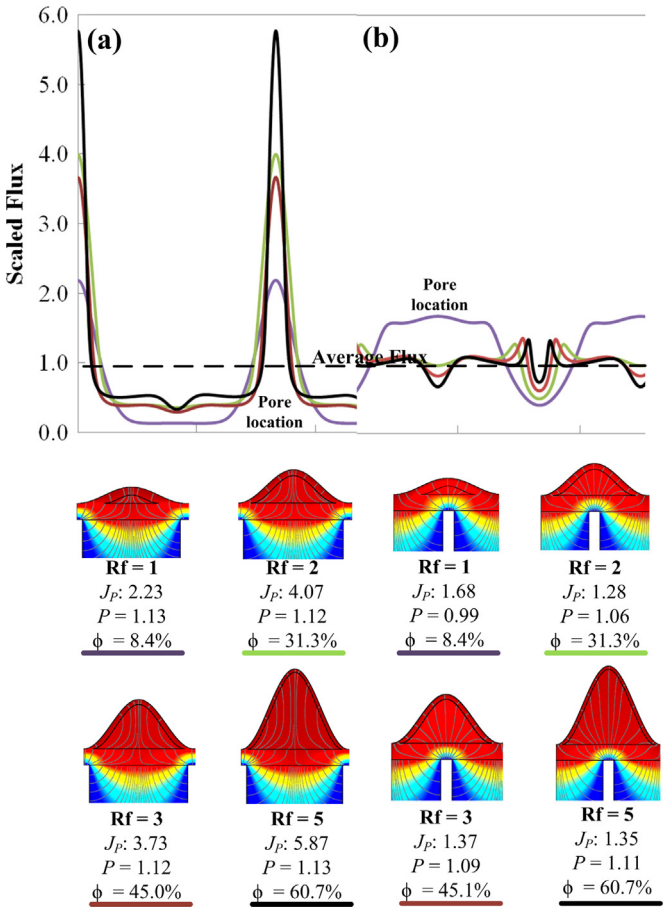

Fig. 10. Supported membranes – proportional void case (see Fig. 3) with varying roughness amplitude. Pores and roughness minima (valley) are either: (a) in-phase (aligned), or (b) out of phase. Top panel shows flux variation plots. Bottom panel shows, for each case, the concentration field, diffusive streamlines and corresponding calculated peak scaled flux, J_P and the permeability P, scaled against that of an equivalent flat thin film with an identical polymer volume.

determining the permeability, but also the flux distribution over the membrane.

When the void volumes are altered in the proportional void scenarios, the flux variation is not as predictable as in the constant void scenarios (see supporting material, Figs. S2 and S3). In the in-phase scenario (Fig. S2), for cases where the void fraction increases by decreasing the thickness of either the base or top films (cases A and B, respectively, in Fig. 4), the highest flux remains at the valleys of the film on top of the pore, resulting in minor changes to the flux distribution. For the case where the void fraction increases by decreasing the thickness of both the base and top films (case C in Fig. 4), although the highest flux is found directly above the support pores, as the void volume increases, the flux variability is reduced since there is less polymer everywhere, resulting in shortened diffusion paths throughout the entire membrane.

For the out-of-phase scenarios, the highest flux regions are no longer on top of the support pores as this is now the thickest part of the film (see Supporting material, Fig. S3). The highest flux regions are in between the ridge and valley regions, since a shorter diffusion path to the pore is provided by the valleys, now aided by the presence of a void. The scaled peak flux hardly changes for case A (decreasing thickness of base film), but increases for case B (decreasing thickness of top film) as the void volume increases. Thus, even though the top film has little effect on changing the permeability of an out-of-phase membrane, it does impact the flux distribution over the membrane. The thinner the top film, the higher the peak flux, J_P. A decrease in the base film thickness increases permeability. When both the top and base film are decreased simultaneously or the entire void volume is increased as in case C, the variability of the flux distribution is exacerbated as the diffusive path directly on top of the pore is shortened compared to other locations in the film.

4.4. Permeability can correlate positively with roughness when voids are present

For the proportional void case with decreasing thickness of base film (case A) in the out-of-phase scenario, the calculated diffusive flux distributions over the membrane segment exhibit insignificant differences in the peak scaled flux, J_P, as shown in Fig. 11 (recall that J_P represents the local flux scaled against the average flux over the segment). When the base film thickness becomes almost negligible (simulation A3 in Fig. 11), it illustrates the possibility of having high permeability with minimal hotspots due to creation of well-distributed, short diffusion paths. In these simulations, we have used a void fraction of $\phi \approx 31\%$, corresponding with our experimental measurements made on commerical membranes. It may be noted that this geometry resembles the image obtained by Kurihara et al. (Fig. 1d) showing thin films with voids having a very thin base film [10], as well as observations that allude to some voids having no base film at all [9,28].

Finally, to demonstrate how surface area affects permeability, modified versions of case A were calculated (denoted by as simulations A4* and A5* in Fig. 11), where the roughness was increased proportionately with the void volume to keep the void fraction constant at $\phi \approx 31\%$. While the permeability increases monotonically with the roughness, or surface area, as shown in Fig. 11b, the flux distribution becomes increasingly uneven as a result (see Fig. 11a). This serves as an illustration of: (1) a case where permeability and roughness will *correlate positively*, since the flux is increased *primarily due to increased membrane surface area*, and (2) the trade-off that exists between roughness-increased permeability and a highly variable flux distribution, leading to a greater occurrence of hot-spots.

4.5. The tradeoff between high permeability and flux 'hot-spots'

In this section we examine the interplay between the flux distribution along a membrane segment and the permeability of the composite structure, as influenced by the presence of voids, roughness amplitude and support pore, as well as their relative locations. Fig. 12 presents the permeability of supported membranes for all previously discussed scenarios plotted against their respective J_P, the scaled peak flux – the ratio between the maximum local flux along a membrane segment and the average flux through the segment. A high scaled peak flux value is indicative of a large variation in flux along the membrane, signifying the presence of potentially fouling-prone flux hot-spots.

As shown in Fig. 12a and c, the in-phase cases (that is, roughness 'valleys' aligned with support pore locations) have much larger flux variation compared to the out-of-phase cases (roughness peaks aligned with pore locations), which means the flux is more evenly distributed when the thin portions of the membrane do not coincide with a pore location (see Fig. 12b and d). Note the inverted trends with roughness; peak flux increases with roughness for the in-phase case, but is reduced by roughness for the out-of-phase case. This is because for in-phase cases, the shortest diffusion paths will always be from the roughness valley to the support pore, creating areas of high flux, while leaving 'dead volumes' of polymer (i.e., the protuberances of the roughness) that barely contribute to transport. On the other hand, for the out-of-phase scenarios, a 'funnel' effect is created whereby the flux is better distributed along the thin film top surface, finding the

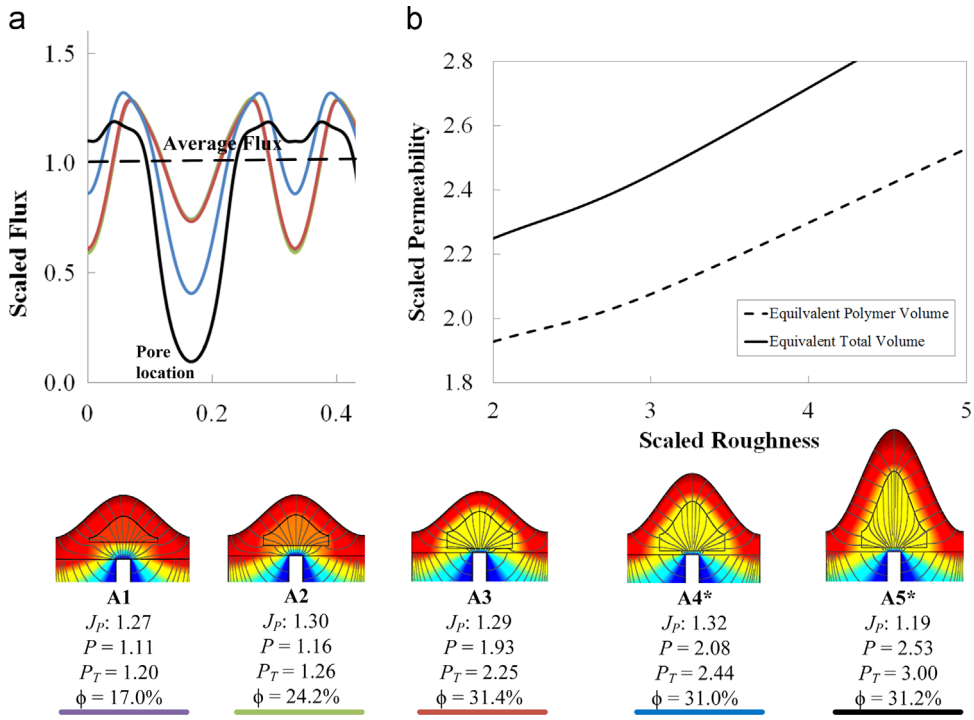

Fig. 11. (a) Scaled flux distribution plot for a segment of an out-of-phase supported membrane-proportional void case with decreasing thickness of base film (case A as described in Fig. 3). (b) Scaled permeability as a function of scaled roughness amplitude with a constant void fraction, for a modified case A. Here, the bottom film is kept at a constant thickness (as in simulation A3). Bottom panel illustrates concentration fields and streamlines of selected simulations where a void is increased at the expense of the bottom film thickness (simulations A1, A2, and A3), and simulations where roughness is increased, with a constant bottom film thickness and nearly constant void fraction (simulations A3, A4*, and A5*). Also shown are the scaled peak flux, J_P, and the permeability scaled using the equivalent polymer volume, P, and the effective total volume, P_T, approaches.

shortest route to the pore. This implies that although a similar permeability can be achieved for a particular membrane, less hotspots - regions prone to fouling - will be obtained if the thin film roughness is out-of-phase with the support. Fig. 12c and d highlight the trend of increased void fraction, illustrating that an increase in permeability invariably occurs in the presence of voids, albeit to a varying extent. As already illustrated in Fig. 11, the greatest improvement in flux, with little change in the peak flux, is achieved for the case where increased void volume is created at the bottom of the active-layer, in an effectively 'thick' region (due to roughness) that occurs over a pore (an out-of-phase case).

5. Conclusions

Transport through a thin-film composite membrane structure (corresponding with fully aromatic polyamide RO/NF membranes) was modeled numerically, with the goal of elucidating the degree to which fluid-filled voids within the active layer impact permeability and flux distributions. Various conceptual geometries of the active and support layers were used which mimicked different scenarios of relative size, content and location of voids in the active layers. TEM images provided evidence supporting the presence of voids in two commercial seawater and brackish water RO membranes, and void fractions in the 30–32% range were estimated through image analysis. Model simulations show that:

- Higher permeability is achieved using the same amount of polymer as in a flat solid film, if the active layer is formed into an undulating film containing voids, due to the creation, on average, of shorter diffusion paths.
- The simulations show that the greatest impact of voids is attained when they are created close to the film-support interface – even at the expense of the base-film. In such cases, the polyamide active layer essentially becomes an undulating film with a very thin, if at all, base-film.
- The morphology of an undulating active layer with a thin base film shows a positive correlation between surface area and flux – in this particular case, increased roughness results in higher permeability, as has been reported for some membranes in the literature; however, the mechanism leading to enhanced flux is not surface area but a shorter average diffusion path through the composite membrane.
- When the membrane roughness peaks are aligned with the support pores ('out-of-phase' configuration), a thicker portion of the active layer on top of a void can dampen the flux distribution, reducing the propensity for high-flux, fouling-prone 'hotspots'.
- By tuning the void fraction and location within the film, the distribution and propensity of hotspots can be tailored and, therefore, permeability may in principle be increased without necessarily resulting in higher fouling propensity, from a hydrodynamic perspective.
- Better control over morphology can potentially ensure that, if hotspots are inevitable, their location may be shifted to areas where cleaning or surface modifications (e.g. polymer grafting) would be easier.

Our results indicate that the water-filled voids within active layers of RO/NF membranes could potentially be tailored to improve water permeability without significantly increasing fouling propensity (from the hydrodynamic perspective, since locally high permeation rates can drive deposition). Thus, further experimental research aimed at controlling void properties (i.e., size, content, location) in the active layer is warranted.

As a final note, we reiterate that while morphological variations

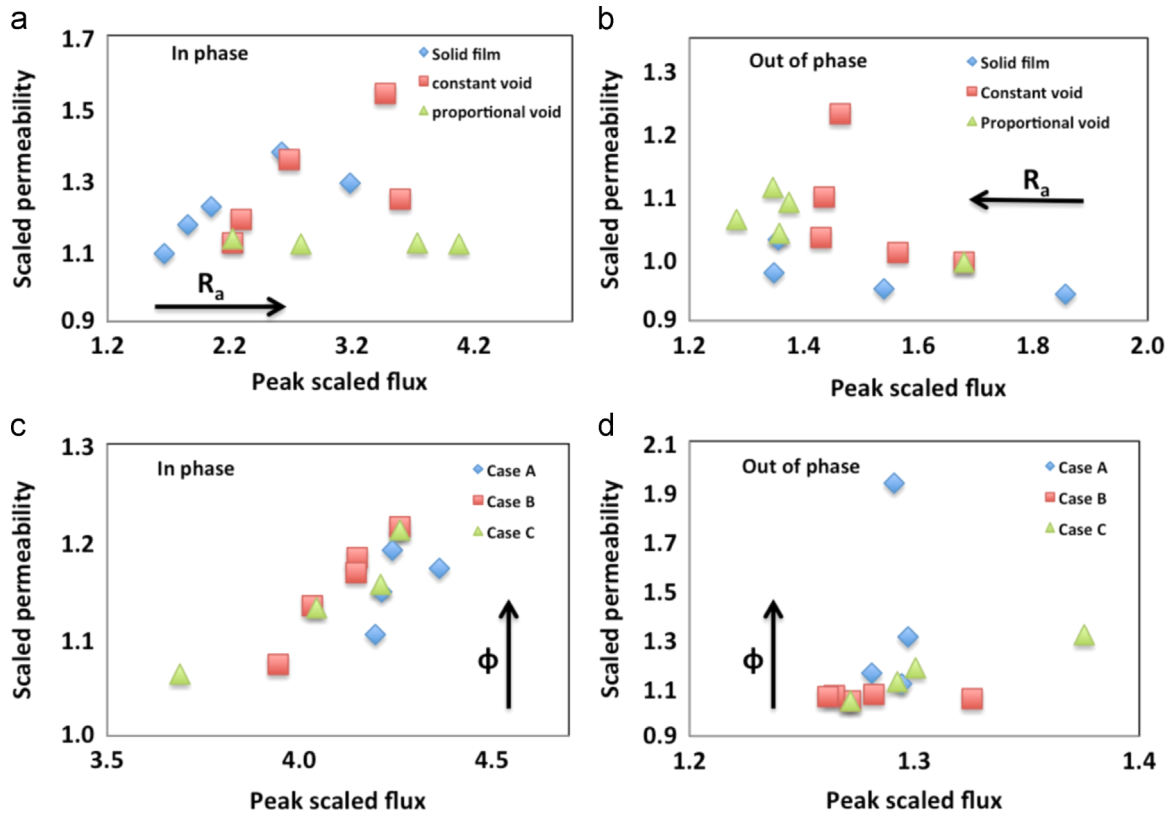

Fig. 12. Phase diagrams of the permeability, scaled against the permeability of a supported flat film with an equivalent polymer volume, shown as a function of the peak scaled flux. In-phase scenarios (roughness minima aligned with support pore locations) are shown in panels (a) and (c). Out-of-phase scenarios (roughness maxima aligned with support pore locations) are shown in panels (b) and (d). Panels (a) and (b) present the permeability of the three morphologies depicted in Fig. 3 (i.e., solid film, constant void and proportional void), with the general increasing trend in scaled roughness amplitude following the marked arrow. Panels (c) and (d) present the permeability of the three morphologies described in Fig. 4 for the proportional void scaling approach (i.e., decreasing thickness of base film, case A; decreasing thickness of top film, case B; decreasing thickness of both base and top film, case C), with the general increasing trend in void fraction following the marked arrow.

are shown to favorably impact permeability, they are coupled to, and are possibly the result of, the polymer chemistry. Understanding this coupling and self-consistently incorporating such effects within a model framework remains an important challenge for future work.

Acknowledgements

M.C.Y.W was supported by the National Science Foundation (NSF) GK-12 Graduate Teaching Fellowship (SEE-LA Award no. 0742410) and UCLA Graduate Division Dissertation Year Fellowship. G.Z.R was supported by a Marie-Curie Grant (No. 275911) from the European Union Seventh Framework Program (FP7/2007-2013). Additional support was provided by the UCLA Department of Civil & Environmental Engineering and the UCLA Henry Samueli School of Engineering & Applied Science. Funding for the experimental work was provided by the National Science Foundation (NSF) Grants Opportunities for Academic Liason with Industry (GOALI) and Chemical and Biological Separations programs under Award#1264690, and NSF Environmental Engineering program under Award#1336532.

Appendix A. Supplementary material

Supplementary data associated with this article can be found in the online version at http://dx.doi.org/10.1016/j.memsci.2015.11.033.

Nomenclature

List of symbols

C_i	species concentration
D_i	diffusion coefficient
J_P	scaled peak flux
P	scaled permeability
R_a	roughness amplitude
R_f	roughness factor, R_a/t_b
t_b	thin film base thickness

Greek letters

∇	gradient operator; $\{\frac{\partial}{\partial X}, \frac{\partial}{\partial Y}\}$
Φ	void fraction

Subscripts

f	film
s	support
v	void

References

[1] J.G. Wijmans, R.W. Baker, The solution-diffusion model: a review, J. Membr.

Sci. 107 (1995) 1–21.
[2] G.Z. Ramon, M.C.Y. Wong, E.M.V. Hoek, Transport through composite membrane, part 1: is there an optimal support membrane? J. Membr. Sci. 415–416 (2012) 298–305.
[3] G.Z. Ramon, E.M.V. Hoek, Transport through composite membranes, part 2: impacts of roughness on permeability and fouling, J. Membr. Sci. 425–426 (2013) 141–148.
[4] M. Bruna, J. Chapman, G.Z. Ramon, The effective flux through a thin-film composite membrane, EuroPhys. Lett. 110 (2015) 40005.
[5] S.H.O. Kim, Positron annihilation spectroscopic evidence to demonstrate the flux-enhancement mechanism in morphology controlled thin-film-composite (TFC) membrane, Environ. Sci. Technol. 39 (2005) 1764–1770.
[6] A.K. Ghosh, B.-H. Jeong, X. Huang, E.M.V. Hoek, Impacts of reaction and curing conditions on polyamide composite reverse osmosis membrane properties, J. Membr. Sci. 311 (2008) 34–45.
[7] M.L. Lind, et al., Influence of zeolite crystal size on zeolite-polyamide thin film nanocomposite membranes, Langmuir 25 (2009) 10139–10145.
[8] W. Xie, et al., Polyamide interfacial composite membranes prepared from m-phenylene diamine, trimesoyl chloride and a new disulfonated diamine, J. Membr. Sci. 403–404 (2012) 152–161.
[9] T. Kamada, T. Ohara, T. Shintani, T. Tsuru, Controlled surface morphology of polyamide membranes via the addition of co-solvent for improved permeate flux, J. Membr. Sci. 467 (2014) 303–312.
[10] L. Lin, R. Lopez, G.Z. Ramon, O. Coronell, Investigating the void structure of the polyamide active layers of thin-film composite membranes, J. Membr. Sci. 497 (2016) 365–376.
[11] M. Hirose, H. Ito, Y. Kamiyama, Effect of skin layer surface structures on the flux behavior of RO membranes, J. Membr. Sci. 121 (1996) 209–215.
[12] S.-yeop Kwak, W.D. Ihm, Use of atomic force microscopy and solid-state NMR spectroscopy to characterize structure-property-performance correlation in high-flux reverse osmosis (RO) membranes, J. Membr. Sci. 158 (1999) 143–153.
[13] S. Madaeni, The effect of surface characteristics on RO membrane performance, Desalination 139 (2001) 371.
[14] A.K. Ghosh, E.M.V. Hoek, Impacts of support membrane structure and chemistry on polyamide polysulfone interfacial composite membranes, J. Membr. Sci. 336 (2009) 140–148.
[15] F.A. Pacheco, I. Pinnau, M. Reinhard, J.O. Leckie, Characterization of isolated polyamide thin films of RO and NF membranes using novel TEM techniques, J. Membr. Sci. 358 (2010) 51–59.
[16] M. Kurihara, M. Hanakawa, Mega-ton Water System: Japanese national research and development project on seawater desalination and wastewater reclamation, Desalination 308 (2013) 131–137.
[17] C. Kong, A. Koushima, T. Kamada, T. Shintani, M. Kanezashi, T. Yoshioka, T. Tsuru, Enhanced performance of inorganic-polyamide nanocomposite membranes prepared by metal-alkoxide-assisted interfacial polymerization, J. Membr. Sci. 366 (2011) 382–388.
[18] Q. An, W.-S. Hung, S.-C. Lo, Y.-H. Li, M. De Guzman, C.-C. Hu, K.-R. Lee, Y.-C. Jean, J.-Y. Lai, Comparison between free volume characteristics of composite membranes fabricated through static and dynamic interfacial polymerization processes, Macromolecules 45 (2012) 3428–3435.
[19] H. Yan, X. Miao, J. Xu, G. Pan, Y. Zhang, Y. Shi, M. Guo, Y. Liu, The porous structure of the fully-aromatic polyamide film in reverse osmosis membranes, J. Membr. Sci. 475 (2015) 504–510.
[20] C. Maxwell, Treatise on Electricity and Magnetism, Oxford University Press, London, UK, 1973.
[21] M. Elimelech, Z. Xiaohua, A.E. Childress, H. Seungkwan, Role of membrane surface morphology in colloidal fouling of cellulose acetate and composite aromatic polyamide reverse osmosis membranes, J. Membr. Sci. 127 (1997) 101–109.
[22] E.M. Vrijenhoek, S. Hong, M. Elimelech, Influence of membrane surface properties on initial rate of colloidal fouling of reverse osmosis and nanofiltration membranes, J. Membr. Sci. 188 (2001) 115–128.
[23] C.C. Mei, B. Vernescu, Homogenization Methods for Multiscale Mechanics, World Scientific, 2010.
[24] C. Tang, Y. Kwon, J.O. Leckie, Effect of membrane chemistry and coating layer on physiochemical properties of thin film composite polyamide RO and NF membranes: I. FTIR and XPS characterization of polyamide and coating layer chemistry, Desalination 242 (2009) 149–167.
[25] S.Y. Kwak, S.G. Jung, Y.S. Yoon, D.W. Ihm, Details of surface features in aromatic polyamide reverse osmosis membranes characterized by scanning electron and atomic force microscopy, J. Polym. Sci. B: Polym. Phys. 37 (1999) 1429–1440.
[26] E.M.V. Hoek, S. Bhattacharjee, M. Elimelech, Effect of membrane roughness on colloid-membrane DLVO interactions, Langmuir 19 (2003) 4836–4847.
[27] G.R. Guillen, T.P. Farrell, R.B. Kaner, E.M.V. Hoek, Pore-structure, hydrophilicity, and particle filtration characteristics of polyaniline–polysulfone ultrafiltration membranes, J. Mater. Chem. 20 (2010) 4621–4628.
[28] C.Y. Tang, Y.-N. Kwon, J.O. Leckie, Probing the nano- and micro-scales of reverse osmosis membranes—a comprehensive characterization of physiochemical properties of uncoated and coated membranes by XPS, TEM, ATR-FTIR, and streaming potential measurements, J. Membr. Sci. 287 (2007) 146–156.
[29] W.S. Rasband, ImageJ, U.S. National Institutes of Health, Bethesda, Maryland, USA, 1997–2014.
[30] C.Y. Tang, Y.-N. Kwon, J.O. Leckie, Characterization of humic acid fouled reverse osmosis and nanofiltration membranes by transmission electron microscopy and streaming potential measurements, Environ. Sci. Technol. 41 (3) (2007) 942–949.